Turk J Phys
31 (2007) , 85 – 96.

Interface and Surface Optical Phonons Spectra in Wurtzite Nitride Quantum Well Wires: Size and Dielectric Effects

Li ZHANG
State Key Laboratory for Mesoscopic Physics, and School of Physics,
Peking University, Beijing 100871, P.R. CHINA
e-mail: zhangli-gz@263.net

Received 28.11.2006

Abstract

By employing the method of electrostatic potential expansion, the interface optical (IO) and surface optical (SO) phonon modes and the corresponding Fröhlich-like electron-phonon-interaction Hamiltonian in a Q1D wurtzite cylindrical quantum well wire (QWW) embedded in nonpolar dielectric matrix are derived and studied based on the dielectric continuum model and Loudon's uniaxial crystal model. Numerical calculations for a wurtzite GaN/AlN QWW are mainly focused on the size- and dielectric-dependent IO and SO phonon spectra and electron-IO (SO)phonons coupling functions. Results reveal that, in general, there are two branches of IO phonon modes and one branch of SO mode in the system. The dispersions of the IO and SO modes are obvious only when the radii ratio β and the dielectric constant of nonpolar matrix ϵ_d is small. The limiting frequencies of IO and SO modes for very large β have been analyzed in depth from both physical and mathematical viewpoints. The reducing behaviors of some modes have been clearly observed. Via the discussion of electrostatic potential spacial distributions of the IO and SO modes, we find that the QWW structures and dielectric constants of nonpolar matrix have little influence on the low-frequency IO mode, but they can greatly affect the potential distributions of high-frequency IO mode and SO mode. Detailed comparison of the dispersion behaviors of the modes and electron-phonon coupling properties in the Q1D wurtzite QWWs with those in wurtzite QWs and cubic quantum dots has also been made. Furthermore, part of the theoretical results derived in the present paper is consistent with the relatively experimental conclusion.

Key Words: Optical Phonon Vibration Spectra; Wurtzite QWW.
PACS: 78.67.Lt; 71.38.-k; 81.05.Ea; 63.20.Kr

1. Introduction

With the rapid progress in nanotechnology of crystal-growth, such as HVPE, MOCVD and MBE, not only cubic Q1D heterostructure, but also wurtzite Q1D quantum-well-wire (QWW) structures have been synthesized [1–5]. The Q1D structures of wurtzite nitride QWW, with wide band-gaps covering from ultraviolet to red, are ideal electronic confined systems for fundamental studies of their physical properties and for the fabrication of high-temperature and high-frequency optoelectronic nanodevices [3–9]. The self-organized wurtzite ZnO and GaN Q1D nanowires ultraviolet lasers have revealed a narrow emission linewidth and relatively low threshold [3–5].

It is well known that, at room and higher temperatures, the scattering of electrons by optical phonons play a dominant role for various electronic properties. The electron-phonon interactions and scattering also govern a number of important properties of quantum heterostructures, including hot-electron relaxation rates, interband transition rates, and room-temperature exciton lifetimes, etc. Hence investigations of polar optical phonon modes and electron-phonon interaction in low-dimensional quantum systems have attracted much interest in theory and experiment [10–27]. One important subject of these studies is the effect of quantum size on the polar optical phonon spectra and electron-phonon coupling properties in these quantum heterostructures [10–18]. The size-dependence of scattering and polaronic effect in GaAs/AlGaAs planar single and multi-layer heterostructure systems have been intensively studied [10, 11, 12]. For example, Chen and coworkers [10] investigated the dispersion of IO modes as a function of the well- and barrier-thickness in semiconductor super-lattices (SLs). Lee et al. [11] and Shi et al. [12] investigated the contributions of various phonon modes (such as IO, LO and half-space modes) to the electron-phonon scattering rates and binding energy and effective mass of polaron in QW systems. Their results revealed that, for neither too wide nor too narrow QWs, the IO modes play very important role in the electron-phonon scattering and polaronic effects. In the case of quite wide or narrow well width, the contributions to the scattering rate and polaronic binding energy will come mainly from the LO modes.

Furthermore, the size-dependence of phonon spectra in quantum dots (QDs) have also been widely reported [13–18]. In experiments, Paula's group [13] studied the phonon spectra of CdTe QDs as a function of the QD size by means of resonant Raman scattering measurements. Their results show that, as the QD size decreases, the SO modes scattering intensity increases, but the electron-phonon coupling decreases. Hwang et al. [14] and Baranov et al. [15] investigated the effect of quantum size on the polar optical phonon modes in CdSe QDs. The blue-shift and broadening of the SO phonon frequency were clearly observed as the QD size was reduced. On the side of theoretical research, Comas and coauthors [16] deduced and analyzed the SO phonon modes in spherical nanostructrued QDs and semiconductor quantum rods under the standard dielectric continuum (DC) approach. Their discussions were mainly focused on the dispersion of SO modes as functions of the QD size and dielectric constants ϵ_d of matrix. Vasilevskiy [17] discussed the dispersion frequency of the dipolar vibrational modes versus the radius in a CdSe QD embedded in different nonpolar matrix. Kanyinda-Malu and Cruz [18] investigated the oscillation spectra of IO and LO phonon modes as a function of the radius in cylindrical QDs.

However, to the best of our knowledge, there is rare work investigating the size and dielectric dependence of polar vibration spectra in Q1D QWW systems, especially for the new synthesized wurtzite QWWs [3–9]. Furthermore, the calculations of electron-phonon scattering and polaronic effects in these Q1D QWW revealed that the effect of quantum-size can greatly influence the scattering rate and binding energy of the polarons in Q1D rectangular QWW [19] and cylindrical QWW [20, 21]. Moreover, due to reduction of the dimensionality and anisotropy of Q1D wurtzite structures, the properties of optical phonon modes in wurtzite QWWs should have more distinct phonon branches [22–27]. Hence it is important and necessary to investigate the size- and dielectric-dependent phonon spectra in Q1D wurtzite QWWs.

In previous studies of polar optical-phonons in wurtzite planar heterostructures, the dielectric continuum (DC) model and Loudon's uniaxial crystal model have been widely adopted [22–28]. As pointed out by Wendler [29], the validity of the DC model is given by two basic facts. First, the Fröhlich type of electron-phonon interaction plays only an important role in the center of the Brillouin zone because only long-wavelength optical phonons produce large polarization fields. And second, the results of microscopic calculations of the optical phonons are in good agreement with those of the DC model. On the other hand, the experimental results of angular dispersion of polar phonons and Raman scattering in wurtzite planar heterostructures have been proven to be in good agreement with the calculations based on Loudon's uniaxial crystal model [30]. Therefore, the DC model and Loudon's uniaxial crystal model will be employed to investigate the IO and SO phonon spectra in the Q1D cylindrical wurtzite QWW system (shown in Figure 1) in the present paper.

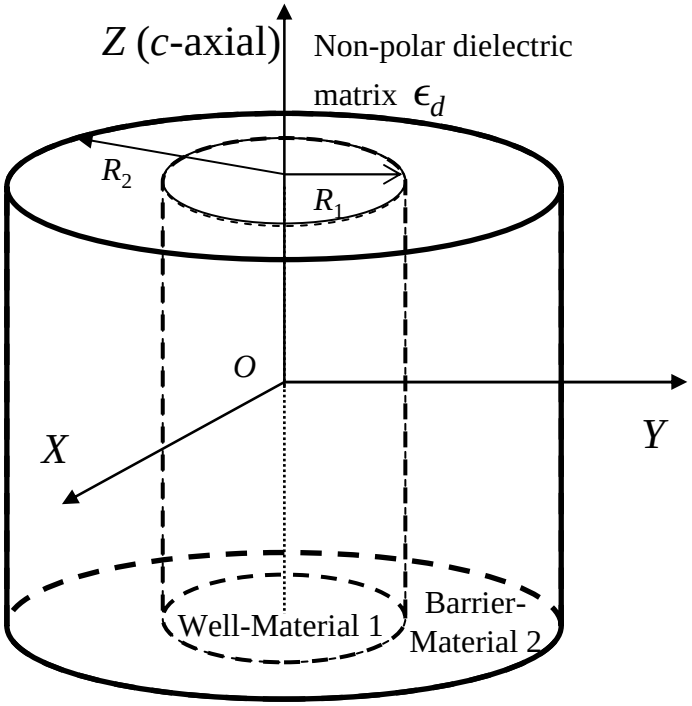

Figure 1. Schematic view of the Q1D wurtzite GaN/AlN cylindrical QWW embedded in nonpolar matrix with dielectric constant ϵ_d.

The main significance of this work embodies the following three points. First, via the method of electrostatic potential expansion, the orthogonality relation for the polarization eigenvector, the dispersion relation equation, the free IO and SO phonon fields as well as the corresponding Fröhlich electron-phonon interaction Hamiltonian in the Q1D wurtzite QWWs have been derived. Secondly, the IO (SO) phonon dispersion as functions of the QWW size, the dielectric constant of the nonpolar surrounding matrix have been numerically calculated and analyzed; the phonon electrostatic potential distributions have also been displayed, and a detailed comparison for these characteristics with those in wurtzite QW and cubic QD systems has been made, and the mathematical and physical origins for these features have been analyzed deeply. Finally, the present theoretical scheme and numerical results are important and useful for further experimental and theoretical investigations of the IO (SO) phonon effects on the complicated Q1D wurtzite QWW structures.

The paper is so organized: the IO and SO phonon dispersion relations and the Fröhlich-like electron-phonon interaction Hamiltonian are deduced in section 2; the numerical results for the dispersion relation, the electron-phonon coupling functions in wurtzite GaN/AlN QWWs are presented and discussed in section 3; At last, we summarized the main results and discussed the significance of the theory described in the current paper in section 4.

2. Theory

Let us consider a wurtzite GaN/AlN QWW model with the inner radius R_1 and the outer radius R_2 placed in nonpolar dielectric environment, as shown in Figure 1, we take the z axis along the direction of the c axis of the wurtzite material and denote the radial directions as t and axial directions as z. In the case of free oscillations (the charge density $\rho_0(\mathbf{r}) = 0$) in the media and via the Maxwell equations, we have the

relation of the electric displacement vector $\mathbf{D}$, and it is given by [24, 27]

$$\begin{aligned}\nabla\cdot\mathbf{D} &= -\nabla^2[\epsilon(\omega)\Phi(\mathbf{r})]\\ &= -\varepsilon_0\left\{\epsilon_t(\omega)\left[\frac{1}{\rho}\frac{\partial}{\partial\rho}(\rho\frac{\partial}{\partial\rho})+\frac{1}{\rho^2}\frac{\partial^2}{\partial\varphi^2}\right]+\epsilon_z(\omega)\frac{\partial^2}{\partial z^2}\right\}\Phi(\mathbf{r})=0,\end{aligned}\tag{1}$$

where $\epsilon(\omega)$ is the dielectric function tensor, and $\Phi(\mathbf{r})$ is the electrostatic potential of polar optical phonons. In order to solve the equation conveniently, we introduce the function $\gamma_i(\omega)$ [27], i.e.,

$$\gamma_i(\omega)=\mathrm{sign}\left[\epsilon_{zi}(\omega)\epsilon_{ti}(\omega)\right]\sqrt{|\epsilon_{zi}(\omega)/\epsilon_{ti}(\omega)|}.\tag{2}$$

Based on the discussion in references [22–28], we know that, when $\gamma_i(\omega)<0$ [i.e., $\epsilon_t(\omega)\epsilon_z(\omega)<0$], the phonon modes correspond to the oscillating waves. On the contrary, they correspond to decaying waves when $\gamma_i(\omega)>0$ [i.e., $\epsilon_t(\omega)\epsilon_z(\omega)>0$]. In terms of the properties of IO and SO phonon modes, we know $\gamma_i(\omega)$ should be position values in all the media constituted the QWW systems. Thus the frequencies of IO and SO phonon modes in the wurtzite GaN/AlN QWWs must fall into the two ranges [22, 26, 27]: $\omega_{t,T1}-\omega_{z,T2}$ and $\omega_{t,L1}-\omega_{z,L2}$. The subscripts 1 and 2 denote the GaN and AlN materials, respectively.

For the IO and SO phonons in a Q1D GaN/AlN wurtzite cylindrical QWW, the solutions of equation (1), i.e., the electrostatic potential of the phonon modes, can be written as

$$\Phi(\mathbf{r})=\sum_{m,k_z}\sum_{i=1}^{3}\mathrm{e}^{\mathrm{i}m\varphi}\mathrm{e}^{\mathrm{i}k_z z}\left[A_iI_m(\gamma_ik_z\rho)+B_iK_m(\gamma_ik_z\rho)\right]\theta(\rho-R_{i-1})\theta(R_i-\rho).\tag{3}$$

In equation (3), $\theta(x)$ is the step function, and $K_m(x)$ and $I_m(x)$ are the first and second kind modified Bessel functions, respectively. Via the boundary conditions (BCs), namely, the continuity of the IO and SO phonon potential functions and their normal components of electric displace at interface $\rho=R_i$ $(i=1,2)$, it is easy to derive the equation

$$\begin{aligned}0 &= -[K_{m-1}(\beta_{32})+K_{m+1}(\beta_{32})]\{\xi_1[I_{m-1}(\beta_{11})+I_{m+1}(\beta_{11})][I_m(\beta_{22})K_m(\beta_{21})\\ &\quad -K_m(\beta_{22})I_m(\beta_{21})]+\xi_2I_m(\beta_{11})[K_m(\beta_{22})[I_{m-1}(\beta_{21})+I_{m+1}(\beta_{21})]\\ &\quad +I_m(\beta_{22})[K_{m-1}(\beta_{21})+K_{m+1}(\beta_{21})]]\}+\xi_2K_m(\beta_{32})\{-[I_{m-1}(\beta_{22})+I_{m+1}(\beta_{22})]\\ &\quad \times[\xi_1[I_{m-1}(\beta_{11})+I_{m+1}(\beta_{11})]K_m(\beta_{21})+\xi_2[K_{m-1}(\beta_{21})+K_{m+1}(\beta_{21})]I_m(\beta_{11})]\\ &\quad +[K_{m-1}(\beta_{22})+K_{m+1}(\beta_{22})][\xi_2I_m(\beta_{11})[I_{m-1}(\beta_{21})+I_{m+1}(\beta_{21})]\\ &\quad -\xi_1I_m(\beta_{21})[I_{m-1}(\beta_{11})+I_{m+1}(\beta_{11})]]\},\end{aligned}\tag{4}$$

where

$$\begin{aligned}\xi_i &= \gamma_i\epsilon_{t,i}\\ \beta_{ij} &= \gamma_ik_zR_j,(i=1,2,3;j=1,2).\end{aligned}\tag{5}$$

Equation (4) just gives the dispersion relation of the IO and SO phonon modes in the Q1D cylindrical wurtzite QWWs. Through the BCs, we also can define the functions $g_i(\omega)$ $(i=1,\,2)$ and $h_i(\omega)$ $(i=2,\,3)$:

$$\begin{aligned}g_1(\omega) &= \xi_2K_m(\beta_{32})\{[I_{m-1}(\beta_{21})+I_{m+1}(\beta_{21})]K_m(\beta_{21})\\ &\quad +[K_{m-1}(\beta_{21})+K_{m+1}(\beta_{21})]I_m(\beta_{21})\},\end{aligned}\tag{6}$$

$$\begin{aligned}g_2(\omega) &= K_m(\beta_{32})\{\xi_1[I_{m-1}(\beta_{11})+I_{m+1}(\beta_{11})]K_m(\beta_{21})\\ &\quad +\xi_2[K_{m-1}(\beta_{21})+K_{m+1}(\beta_{21})]I_m(\beta_{11})\},\end{aligned}\tag{7}$$

$$\begin{aligned} h_2(\omega) &= \xi_2 I_m(\beta_{11})[I_{m-1}(\beta_{21}) + I_{m+1}(\beta_{21})] \\ &\quad -\xi_1 I_m(\beta_{21})[I_{m-1}(\beta_{11}) + I_{m+1}(\beta_{11})], \end{aligned} \tag{8}$$

$$\begin{aligned} h_3(\omega) &= \xi_1[I_{m-1}(\beta_{11}) + I_{m+1}(\beta_{11})][I_m(\beta_{22})K_m(\beta_{21}) - I_m(\beta_{21})K_m(\beta_{22})] \\ &\quad +\xi_2 I_m(\beta_{11})\{[I_{m-1}(\beta_{21}) + I_{m+1}(\beta_{21})]K_m(\beta_{22}) \\ &\quad +[K_{m-1}(\beta_{21}) + K_{m+1}(\beta_{21})]I_m(\beta_{22})\}. \end{aligned} \tag{9}$$

By using the defined functions $g_i(\omega)$ $(i = 1, 2)$ and $h_i(\omega)$ $(i = 2, 3)$, the phonon potential function (3) can be further rewritten as

$$\Phi(\mathbf{r}) = A_1 \sum_{m,k_z} \sum_{i=1}^{3} \mathrm{e}^{\mathrm{i}m\varphi} \mathrm{e}^{\mathrm{i}k_z z} \left[g_i I_m(\gamma_i k_z \rho) + h_i K_m(\gamma_i k_z \rho) \right] \theta(\rho - R_{i-1}) \theta(R_i - \rho). \tag{10}$$

Via Eq. (10), the polarization fields for the IO (SO) phonon modes of the system are given by

$$\begin{aligned} \mathbf{P}_{mk_z}^{\mathrm{IO,SO}} &= \frac{A_1}{4\pi} \mathrm{e}^{\mathrm{i}m\varphi} \mathrm{e}^{\mathrm{i}k_z z} \sum_{i=1}^{3} \{ \frac{1}{2}(1 - \epsilon_{t,i})\gamma_i k_z [g_i(\omega)[I_{m-1}(\gamma_i k_z \rho) + I_{m+1}(\gamma_i k_z \rho)] \\ &\quad -h_i(\omega)[K_{m-1}(\gamma_i k_z \rho) + K_{m+1}(\gamma_i k_z \rho)]]\widehat{\rho} + (1 - \epsilon_{t,i}) \frac{\mathrm{i}m}{\rho} [g_i(\omega) I_m(\gamma_i k_z \rho) \\ &\quad +h_i(\omega) K_m(\gamma_i k_z \rho)]\widehat{\varphi} + \mathrm{i}(1 - \epsilon_{z,i}) k_z [g_i(\omega) I_m(\gamma_i k_z \rho) + h_i(\omega) K_m(\gamma_i k_z \rho)]\widehat{z}\}, \end{aligned} \tag{11}$$

Then we can obtain the orthogonality relation for $\mathbf{P}_{mk_z}^{\mathrm{IO,SO}}$, and it is given as

$$\begin{aligned} &\int \mathbf{P}_{m'k_z'}^{\mathrm{IO,SO}^*} \cdot \mathbf{P}_{mk_z}^{\mathrm{IO,SO}} \mathrm{d}^3\mathbf{r} \\ &= \frac{A_1^2 k_z^2 L}{16\pi} \left\{ \int_0^{R_1} \rho \mathrm{d}\rho [2(1 - \epsilon_{z,1})^2 g_1^2 I_m^2(\gamma_1 k_z \rho) + \gamma_1^2 (1 - \epsilon_{t,1})^2 g_1^2 [I_{m-1}^2(\gamma_1 k_z \rho) + I_{m+1}^2(\gamma_1 k_z \rho)]] \right. \\ &\quad + \int_{R_1}^{R_2} \rho \mathrm{d}\rho \{ (1 - \epsilon_{z,2})^2 [2 g_2^2 I_m^2(\gamma_2 k_z \rho) + 2 h_2^2 K_m^2(\gamma_2 k_z \rho) + 4 g_2 h_2 I_m(\gamma_2 k_z \rho) K_m(\gamma_2 k_z \rho)] \\ &\quad +\gamma_2^2 (1 - \epsilon_{t,2})^2 [g_2^2 (I_{m-1}^2(\gamma_2 k_z \rho) + I_{m+1}^2(\gamma_2 k_z \rho)) + h_2^2 (K_{m-1}^2(\gamma_2 k_z \rho) + K_{m+1}^2(\gamma_2 k_z \rho)) \\ &\quad \left. +2 g_2 h_2 (I_{m+1}(\gamma_2 k_z \rho) K_{m+1}(\gamma_2 k_z \rho) - I_{m-1}(\gamma_2 k_z \rho) K_{m-1}(\gamma_2 k_z \rho))] \} \right\} \delta_{m'm} \delta_{k_z' k_z}, \end{aligned} \tag{12}$$

where L is the length of the QWW. The Hamiltonian for the IO and SO phonon modes in wurtzite QWW is read as [27]

$$\begin{aligned} H_{\mathrm{IO,SO}} &= \frac{n^* \mu}{2} \int \left[\left(\frac{1}{n^* e_t [1 + (\alpha_t \mu / e_t^2)(\omega_{0t}^2 - \omega^2)]} \right)^2 \left(\dot{\mathbf{P}}_t^* \cdot \dot{\mathbf{P}}_t + \omega^2 \mathbf{P}_t^* \cdot \mathbf{P}_t \right) \right. \\ &\quad \left. + \left(\frac{1}{n^* e_z [1 + (\alpha_t \mu / e_z^2)(\omega_{0z}^2 - \omega^2)]} \right)^2 \left(\dot{P}_z^* \cdot \dot{P}_z + \omega^2 P_z^* \cdot P_z \right) \right] \mathrm{d}^3\mathbf{r}, \end{aligned} \tag{13}$$

where μ is the reduced mass of the ion pair and n^* is the number of ion pairs per unit volume, ω_{0t} and ω_{0z} are the frequencies associated with the short-range force between ions, e_t and e_z are the effective charges of the ions, α_t and α_z are the electronic polarizabilities per ion pair along the t and z directions, respectively. Based on the orthogonality relation of the polarization vector (12) and choosing

$$\begin{aligned} |A_1|^{-2} &= \frac{k_z^2 L}{2\omega^2} \{ \int_0^{R_1} \rho \mathrm{d}\rho [2\overline{\epsilon}_{z,1} g_1^2 I_m^2(\gamma_1 k_z \rho) + \gamma_1^2 \overline{\epsilon}_{t,1} g_1^2 [I_{m-1}^2(\gamma_1 k_z \rho) + I_{m+1}^2(\gamma_1 k_z \rho)]] \\ &\quad + \int_{R_1}^{R_2} \rho \mathrm{d}\rho \{ \overline{\epsilon}_{z,2} [2 g_2^2 I_m^2(\gamma_2 k_z \rho) + 2 h_2^2 K_m^2(\gamma_2 k_z \rho) + 4 g_2 h_2 I_m(\gamma_2 k_z \rho) K_m(\gamma_2 k_z \rho)] \\ &\quad +\gamma_2^2 \overline{\epsilon}_{t,2} [g_2^2 (I_{m-1}^2(\gamma_2 k_z \rho) + I_{m+1}^2(\gamma_2 k_z \rho)) + h_2^2 (K_{m-1}^2(\gamma_2 k_z \rho) + K_{m+1}^2(\gamma_2 k_z \rho)) \\ &\quad +2 g_2 h_2 (I_{m+1}(\gamma_2 k_z \rho) K_{m+1}(\gamma_2 k_z \rho) - I_{m-1}(\gamma_2 k_z \rho) K_{m-1}(\gamma_2 k_z \rho))] \}, \end{aligned} \tag{14}$$

$\mathbf{P}^{\mathrm{IO,SO}}_{mk_z}$ can be treated as an orthogonal and complete set, which can be used to express the free IO and SO phonon field $H_{\mathrm{IO,SO}}$ and the electron-phonon interaction Hamiltonian $H_{e-\mathrm{IO,SO}}$. In Eq. (14), $\overline{\epsilon}_{u,i}$ is the effective dielectric function of the ith-layer material, which is defined as

$$\overline{\epsilon}_{u,i} = \left(\frac{1}{\epsilon_{u,i} - \epsilon_{u,i0}} - \frac{1}{\epsilon_{u,i} - \epsilon_{u,i\infty}} \right)^{-1}, u = t, z; i = 1, 2. \tag{15}$$

The free IO and SO phonon field is given by

$$H_{\mathrm{IO,SO}} = \sum_{m,k_z} \hbar\omega \left[b^{\dagger}_m(k_z) b_m(k_z) + \frac{1}{2} \right], \tag{16}$$

where $b^{\dagger}_m(k_z)$ and $b_m(k_z)$ are creation and annihilation boson operators for IO and SO phonons of the (m, k_z)-th mode. The Fröhlich-like Hamiltonian describing the interaction between an electron and the IO (SO) phonons is given by

$$H_{e-\mathrm{IO,SO}} = -\sum_{m,k_z} \Gamma^{\mathrm{IO,SO}}_{m,k_z R_1}(\rho)[b_m(k_z)\mathrm{e}^{\mathrm{i}m\varphi}\mathrm{e}^{\mathrm{i}k_z z} + \mathrm{H.c.}], \tag{17}$$

where $\Gamma^{\mathrm{IO,SO}}_{m,k_z R_1}(\rho)$ is the electron-phonon coupling function, which describes the coupling strength of a single electron at the position ρ with the (m, k_z)-th IO (SO) mode, and is defined as

$$\Gamma^{\mathrm{IO,SO}}_{m,k_z R_1}(\rho) = N_m \times \begin{cases} g_1(\omega) I_m(\gamma_1 k_z \rho) & \rho \leqslant R_1 \\ g_2(\omega) I_m(\gamma_2 k_z \rho) + h_2(\omega) K_m(\gamma_2 k_z \rho) & R_1 < \rho \leqslant R_2 \\ h_3(\omega) K_m(\gamma_3 k_z \rho) & \rho > R_2 \end{cases} \tag{18}$$

with

$$|N_m| = \sqrt{\frac{\hbar e^2}{\omega}} |A_1|. \tag{19}$$

3. Numerical Results and Discussion

In this section, we have presented the numerical results of polar oscillation spectra and the distributions of the electrostatic potentials of the IO (SO) phonon modes in a Q1D GaN/AlN wurtzite QWW with the inner radius of $R_1 = 5$ nm. In the discussion, we laid emphasis on the influence of QWW structure ($\beta = R_2/R_1$) and dielectric matrix (ϵ_d) on the dispersion frequencies and electron-phonon coupling functions. The material parameters used in our calculations originated from reference [22]

Figure 2 shows the dispersion frequencies $\hbar\omega$ of the IO and SO phonon modes as a function of the ratio of inner and outer radii β in the wurtzite QWW system with different azimuthal number m and wave-number in z- direction k_z. The dielectric constant of nonpolar matrix ϵ_d is kept at 1. From the figure, it can be seen that, for a definite QWW structure β, and given azimuthal quantum m and wave-number k_z, there are three branches of IO and SO phonon modes in general. This means that equation (4) usually has three solutions for ω. These modes are labeled by 1, 2 and 3 in terms of the order of increasing frequency. Modes 1 and 3 are monotonic and degressive functions of β, while mode 2 is the monotonic and incremental function of β. It is also noticed that the frequency of the low-frequency mode 1 vary between ω_{tT1} and ω_{zT2}, and those of the high-frequency modes 2 and 3 fall into the range of ω_{tL1} to ω_{zL2}, which is completely consistent with the case in wurtzite QW systems [22]. When β is small, the dispersions are more obvious. The dispersions of these modes nearly could be neglected when $\beta > 5$. An obviously different feature from the situation of structural- dependent IO phonon spectra in cubic QD [16, 18] is that, some modes, such as modes 2 and 3 with $m = 0$ and $k_z = 1/R_1$ (Figure 2(a)) in the Q1D wurtzite QWW, can only appear when $\beta \geqslant 1.23$ and $\beta \geqslant 2.1$, respectively. But in the cubic crystal QDs, all of the IO modes always exist, even for very

little radius and aspect ratio [16, 18]. This characteristic is completely due to the anisotropy of wurtzite crystals. Detailed calculations show that the modes 2 and 3 in Figure 2(a) occur at the frequencies 91.832 meV and 110.09 meV, which are very close to the two characteristic frequencies $\omega_{z,L2}$ and $\omega_{t,L1}$, respectively. Once $\omega > \omega_{z,L2}$ or $\omega < \omega_{t,L1}$, $\gamma_i(\omega)$ will change to be a negative number and the IO (SO) phonon modes will reduce to the other oscillating phonon modes, such as confined modes, quasi-confined modes [22] or propagating modes [23]. Another special feature for mode 1 with $m = 0$ and $k_z = 1/R_1$ (Figure 2(a)) is that, IO mode 1 will disappear when β is over 1.5. We can see from Figure 2(a), when $\beta \to 1.5$, the frequency of mode 1 approach 69.26 meV, which is very close to the characteristic frequency $\omega_{t,T1}$. Hence the reduced behavior of mode 1 from IO mode to other oscillating mode will occur once $\beta > 1.5$.

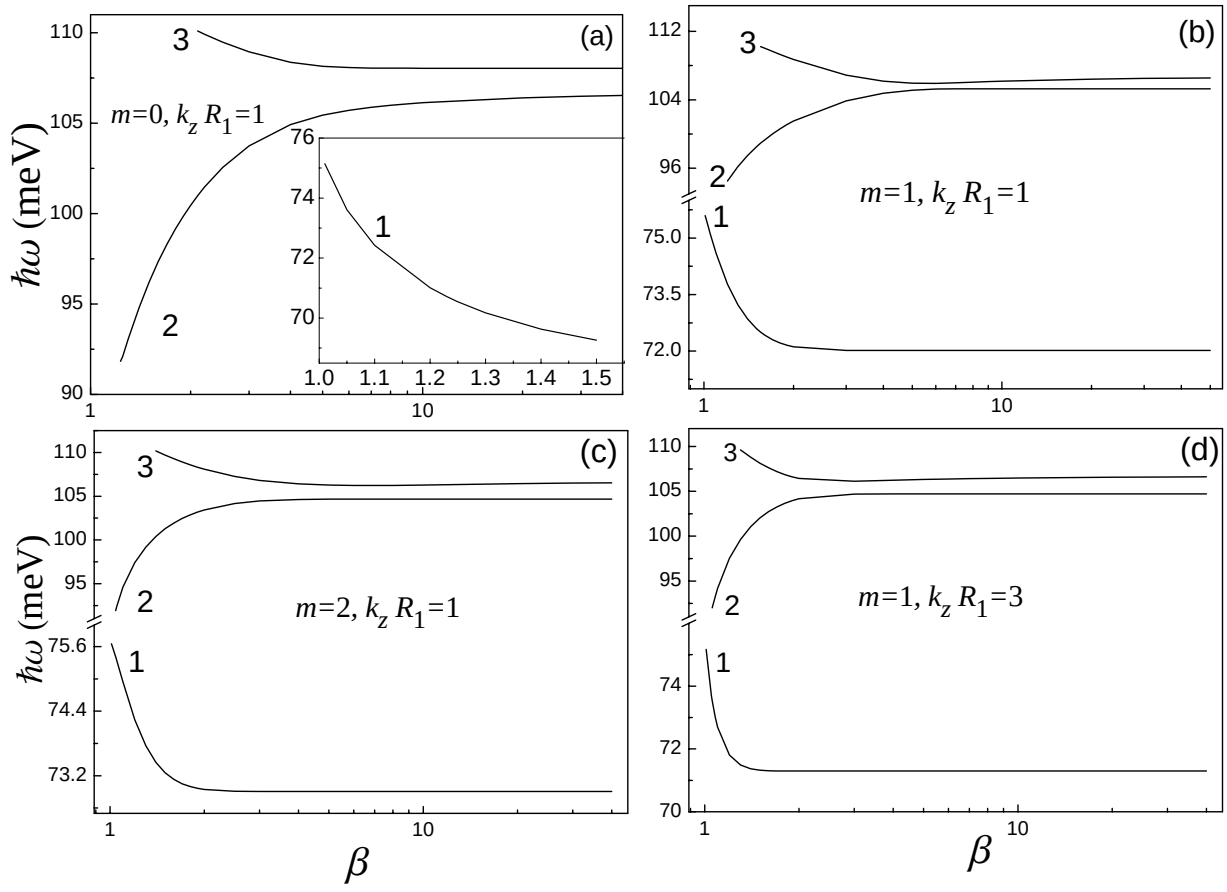

Figure 2. The dispersion frequencies $\hbar\omega$ of the IO and SO phonon modes as a functions of the radius ratio β in the wurtzite QWW system with dielectric constant $\epsilon_d = 1$.

In order to label and compare these branches of IO and SO modes, we computed and analyzed the limiting frequencies of these modes for $\beta \to \infty$. In fact, these limiting frequency values are just the solutions of the dispersion equation of IO phonon modes in wurtzite single cylindrical heterostructure [27], i.e.,

$$\begin{aligned} & \epsilon_{t,1}\gamma_1 K_m(\gamma_2 k_z R)[I_{m-1}(\gamma_1 k_z R) + I_{m+1}(\gamma_1 k_z R)] \\ = \; & -\epsilon_{t,2}\gamma_2 I_m(\gamma_1 k_z R)[K_{m-1}(\gamma_2 k_z R) + K_{m+1}(\gamma_2 k_z R)]. \end{aligned} \tag{20}$$

This interesting characteristic is not accidental, but has profound physical origins. It is well known that, in coupling low-dimensional quantum systems, the electrostatic potential coupling of IO modes on the interfaces is very strong when the distances between the interfaces is not large enough. With the increase

of interface distances, this coupling will become weaker and weaker. As the distance approaches infinity, the electrostatic potentials of IO modes will be completely decoupled. Thus the limiting frequencies of the IO and SO modes in GaN/AlN QWW embedded in nonpolar matrix for very large β will be determined only by the single wurtzite cylindrical heterostructures [27], i.e., GaN/AlN and AlN/Matrix(ϵ_d). Therefore, dispersion equation (20) just gives the limiting frequency values of IO and SO modes for large β in our Q1D wurtzite QWWs. Via detailed calculation, it is found there are two branches of IO modes at the interface $\rho = R_1$, and only one branch of SO mode is localized at the surface $\rho = R_2$. As can be seen more clearly in Figures 3 and 4, mode 1 is the IO mode at the interface $\rho = R_1$, but the case for modes 2 and 3 has little difference. When k_z is little (such as $k_z R_1 \leqslant 1$ in Figures 3), mode 3 can be looked on as the the IO mode at $\rho = R_1$, and mode 2 can be treated as the the SO mode at $\rho = R_2$. But when k_z is relatively large (such as $k_z R_1 \geqslant 3$ in Figure 4), the situation is just opposite, i.e., mode 2 acts as the the IO mode at $\rho = R_1$, and mode 3 become the the SO mode at $\rho = R_2$. Even so, there always exists two branches of IO modes, and only one branch of SO mode in the QWW systems regarding of large and little wave-number k_z in general. Comparing Figures 2(a)–2(c), we find that, with the increase of m, the limited frequency values of modes 2 and 3 have obvious decrease, whereas that of mode 1 has obvious increase. Comparing Figure 2(b) with Figure 2(d), it is also observed that, as k_z increases, the limited values of modes 1 and 2 have little increase, whereas that of mode 3 has little increase. This observation is consistent qualitatively with the results in reference [27].

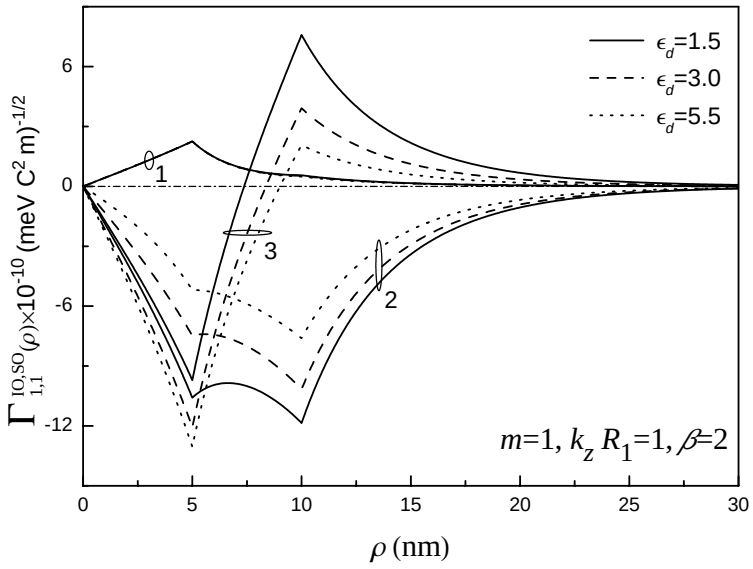

Figure 3. The electron-phonon coupling function $\Gamma^{\mathrm{IO,SO}}_{m,k_z R_1}(\rho)$ as a function of ρ in the wurtzite QWWs embedded in three dielectric constants of matrix, $\epsilon_d = 1.5$ (solid line), 3 (dash line) and 5.5 (dot line), respectively.

In Figure 5, we present the frequencies $\hbar\omega$ of IO and SO phonons as a function of dielectric constant of the nonpolar matrix ϵ_d for the wurtzite QWW with a definite structure $\beta = 2$. Of course, the azimuthal quantum number m and wave-number k_z are kept at define values 1 and $1/R_1$, respectively. We observe that mode 3 has little dispersion, i.e., the frequency of mode 3 decreases from 108.701 meV to 106.497 meV as ϵ_d increases from 1 to 10. Furthermore, the dispersion of mode 1 nearly could be ignored. The frequency dispersion for mode 2 is most obvious among the three branches of modes. In fact, in the case of $m = 1$ and $k_z R_1 = 1$ (refer to the discussion for Figure 2), the modes 1 and 3 act as the IO modes whose potentials are mainly localized at the interface, while mode 2 is the SO mode whose potential localized mainly at the surface, which can be seen quite clearly in Figure 3. Hence it is natural that the influence of the dielectric constant ϵ_d on the SO mode is stronger than that on the IO modes. On the other hand, the curve of mode

2 is cut off at about $\epsilon_d = 5.8$. This is also an interesting feature due to anisotropic wurtzite heterostructure, and it was not observed in isotropic semiconductor heterostructure [16], even for $\epsilon_d \to 10$. This behavior of the SO mode 2 can be understood qualitatively from the case of planar AlN/Matrix(ϵ_d) heterostructure [22]. Similar to the case of single wurtzite planar heterostructure, the IO phonon frequency in planar AlN/Matrix heterostructure can be solved by the equation $\sqrt{|\epsilon_{t,2}(\omega)\epsilon_{z,2}(\omega)|} = \epsilon_d$. The function $\sqrt{|\epsilon_{t,2}(\omega)\epsilon_{z,2}(\omega)|}$ is a monotonic and degressive function of ω in the frequency range $\omega_{tL1} - \omega_{zL2}$. Thus the frequency of SO mode decrease with the increase of dielectric constant ϵ_d. When $\epsilon_d \to 5.8$, the SO mode frequency approaches the characteristics frequency ω_{tL1}. It is known from the above discussion, once $\omega < \omega_{tL1}$, the function $\gamma_2(\omega)$ becomes negative, and thus the SO mode cannot exist in the situation and must reduce to the other oscillating modes, such as quasi-confined modes or half-space modes [22–26].

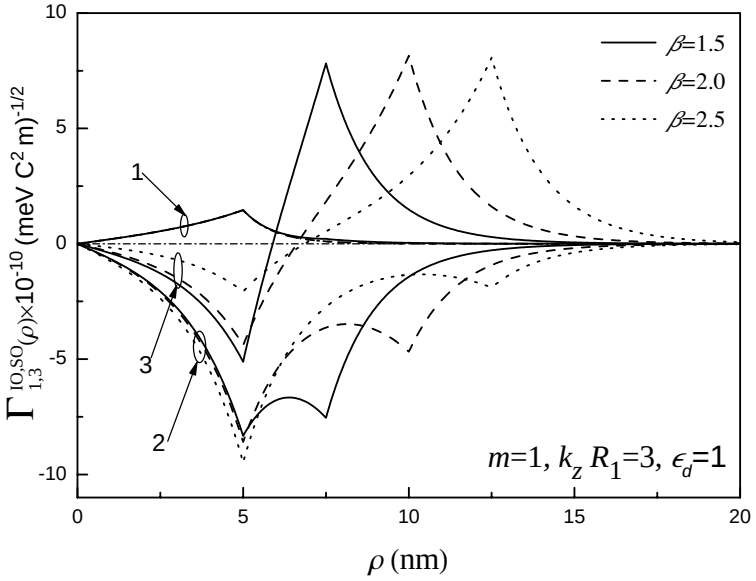

Figure 4. The electron-phonon coupling function $\Gamma^{\mathrm{IO,SO}}_{m,k_z R_1}(\rho)$ as a function of ρ for three different wurtzite QWW structures with $\beta = 1.5$ (solid line), 2 (dash line) and 2.5 (dot line), respectively.

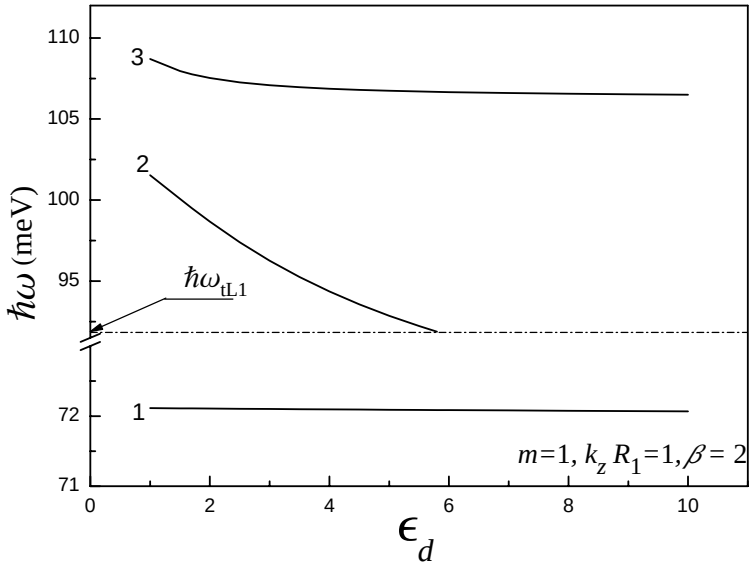

Figure 5. The frequencies $\hbar\omega$ of IO and SO phonons as a function of dielectric constant of the nonpolar matrix ϵ_d for the wurtzite QWW with $\beta = 2$.

Next, we further investigate the electron-phonon coupling function $\Gamma^{\mathrm{IO,SO}}_{m,k_zR_1}(\rho)$ whose features may be helpful for understanding the electron-phonon coupling strength and the electrostatic potential distribution of the IO (SO) phonon modes in the wurtzite QWWs. Figure 3 depicts the coupling function $\Gamma^{\mathrm{IO,SO}}_{m,k_zR_1}(\rho)$ as a function of ρ when $m = k_zR_1 = 1$ and $\beta = 2$. The solid, dash and dot lines correspond to three different dielectric constants of matrix, $\epsilon_d = 1.5$, 3 and 5.5, respectively. Via the figure, it is seen that modes 1 and 3 are mainly localized at the first interface $\rho = R_1$, and mode 1 mainly at the surface $\rho = R_2$. So the modes 1 and 3 can be looked on as the IO modes at the first interface, while the mode 2 can be treated as the SO modes at the surface, which are completely consistent with the analysis for Figure 5. As ϵ_d increases, the electrostatic potential distribution of IO mode 1 is basically kept unchanged, which could be understood directly from the nondispersive property of the mode on ϵ_d (refer to Figure 5). But the dielectric constant has great influence on the potentials of modes 2 and 3. The maximum values of $\Gamma^{\mathrm{IO,SO}}_{m,k_zR_1}(\rho)$ of the IO mode 3 remarkably increase, whereas those of the SO mode 2 notably decrease with the increasing ϵ_d. We also notice that the high frequency branch relative to the low frequency one plays more important role in the electron-phonons interactions, which differs obviously from the case in wurtzite QWs due to their different confined dimensions [22].

In Figure 4, we also show the spacial distributions of the coupling function $\Gamma^{\mathrm{IO,SO}}_{m,k_zR_1}(\rho)$. The solid, dash and dot lines correspond to three different wurtzite QWW structures with $\beta = 1.5$, 2 and 2.5, respectively. The azimuthal quantum number m, wave-number k_zR_1 and dielectric constant ϵ_d are fixed at 1, 3 and 1, respectively. Similar to the case in Figure 3, mode 1 is mainly localized at the interface, and its potential is not affected nearly by the change in QWW structures. Comparing with Figure 3, we find that modes 2 and 3 exchange their localizing positions with each other in Figure 4, namely, mode 2 is the IO mode, and mode 3 act as the SO mode. This just proves the above analysis in Figure 2 regarding the exchange behavior of modes 2 and 3 due to the different free wave-numbers k_z. Furthermore, it is also observed the strength of electron-phonon coupling for modes 2 and 3 have obvious enhancement as β increases. This result is consistent with the Paula's experimental conclusion in CdTe QD [13], i.e. decrease in the electron-phonon coupling as the nanocrystal size is decreased.

4. Summary and Conclusions

Within the framework of the DC model and Loudon's uniaxial crystal model [28], the IO and SO phonon modes, the orthogonality relation for polarization eigenvector, the dispersion relation, and Fröhlich electron-phonon interaction Hamiltonian in a Q1D wurtzite cylindrical QWW systems have been deduced and studied in the present paper. Numerical calculations on a GaN/AlN QWW have been performed, and the calculations are mainly focused on the size- and dielectric-dependent IO and SO phonon spectra and the electron-phonon coupling functions. Results reveal that, in general, there exists two branches of IO modes and one branch of SO mode in the Q1D wurtzite QWW. The dispersions of IO and SO phonon modes is more obvious when β and ϵ_d is small, and the dispersions of some modes almost could be neglected for relatively large β and ϵ_d. Furthermore, the limiting frequencies of IO and SO modes for very large β have been analyzed in depth from both of physical and mathematical viewpoints. The reducing behaviors of some IO and SO modes have been clearly observed. Via the discussion of the electron-phonon coupling functions, it is found that the wurtzite QWW structures and dielectric constants of nonpolar matrix have little influence on the low-frequency IO mode, but they can greatly affect the potential distributions of high-frequency IO mode and SO mode. With the increase of dielectric constant of matrix ϵ_d, the electron-phonon coupling strength of high-frequency IO mode is enhanced apparently; but that of SO mode is decreased obviously. As β increases, both the coupling strengths of SO mode and high-frequency IO mode have enhancements, and this feature is completely consistent with the relatively experimental results [13].

The theoretical results obtained in present paper are important and useful for further experimental and theoretical investigation of the size- and dielectric-dependent phonon spectra and electron-phonon in-

teractions, as well as for device applications in Q1D wurtzite QWW systems. We hope that the present work will stimulate further investigations of the lattice dynamical properties, and guide and explain relative experimental phenomenons in the Q1D wurtzite semiconductor heterostructure systems.

Acknowledgments

We would like to acknowledge the detailed and valuable instructs of Prof. J. J. Shi. This work was supported by the Science and Technology Project of Advanced Academy of Guangzhou City under Grant No. 2060, Peoples Republic of China.

References

[1] K. Suenaga, C. Colliex, N. Demoncy, A. Loiseau, H. Pascard, and F. Willaime, *Science*, **278**, (1997), 653; Y. Zhang, K. Suenaga, C. Colliex, and S. Iijima, *Science*, **281**, (1998), 973.

[2] L. J. Lauhon, M. S. Gudlksen, D. Wang, and C. M. Lieber, *Nature*, **420**, (2002), 57.

[3] H-J. Choi, J. C. Johnson, R. He, S-K. Lee, F. Kim, P. Pauzauskie, J. Goldberger, R.J. Saykally, and P. Yang, *J. Phys. Chem.*, **B107**, (2003), 8271.

[4] J. Goldberger, R. He, Y. Zhang, S. Lee, H. Yan, H-J. Choi, and P. Yang, *Nature*, **422**, (2003), 599.

[5] M. H. Huang, S. Mao, H. Fieck, H. Yan, Y. Wu, H. Kind, E. Weber, R. Richard, and P. Yang, *Science*, **292**, (2001), 5523.

[6] W. Huang, and F. Jain, *J. Appl. Phys.*, **87**, (2000), 7354.

[7] Y. Kawakami, N. Higashimaki, K. Doi, K. Nakamura, and A. Tachibana, *Phys. Status Solidi (c)*, **0**, (2003), 2318.

[8] J-R. Kim, B-K. Kim, I.J. Lee, and J-J. Kim, *Phys. Rev.*, **B69**, (2004), 233303.

[9] H-L. Liu, C. C. Chen, C-T. Chia, C. C. Yeh, C-H. Chen, M-Y. Yu, S. Keller, and S.P. DenBaars, *Chem. Phys. Lett.*, **345**, (2001), 245.

[10] K. Q. Chen, W. H. Duan, W. X. Li, J. Wu, H. Y. Wang, and B. L. Gu, *Microelectronic Engineering*, **66**, (2003), 26; K.Q. Chen, W. H. Duan, B. L. Gu, and B. Y. Gu, *Phys. Lett. A*, **299**, (2002), 634; K. Q. Chen, W. H. Duan, J. Wu, B. L. Gu, and B. Y. Gu, *J. Phys.: Condens. Matter*, **14**, (2002), 13761.

[11] H. C. Lee, K. W. Sun, and C. P. Lee, *J. Appl. Phys.*, **92**, (2002), 268.

[12] J. J. Shi, and S. H. Pan, *Phys. Rev.*, **B51**, (1995), 17681; J. J. Shi, X. Q. Zhu, Z. X. Liu, S. H. Pan, and X. Y. Li, *Phys. Rev.*, **B55**, (1997), 4680.

[13] A. M. de Paula, L. C. Barbosa, C. H. B. Cruz, O. L. Alves, J. A. Sanjurjo, and C. L. Cesar, *Appl. Phys. Lett.*, **69**, (1996), 357; *Supperlattices and Microstructures*, **23**, (1998), 1103.

[14] Y-N. Hwang, and S-H. Park, *Phys. Rev.*, **B59**, (1999), 7258.

[15] A. V. Baranov, Y. P. Rakovich, J. F. Donegan, T. S. Perova, R. A. Moore, D. V. Talapin, A. L. Rogach, Y. Masumoto, and I. Nabiev, *Phys. Rev.*, **B68**, (2003), 165306.

[16] F. Comas, N. Studart, and G. E. Marques, *Solid State Commun.*, **130**, (2004), 477; F. Comas, and A. Odriazola, *Phys. Stat. Sol. (b)*, **242**, (2005), 1267.

[17] M. I. Vasilevskiy, *Phys. Rev.*, **B66**, (2002), 195326.

[18] C. Kanyinda-Malu, and R. M. de la Cruz, *Phys. Rev.*, **B59**, (1999), 1621.

[19] K. W. Kim, M. A. Stroscio, A. Bhatt, R. Mickevicius, and V.V. Mitin, *J. Appl. Phys.*, **70**, (1991), 319.

[20] H. J. Xie, C. Y. Chen, and B. K. Ma, *Phys. Rev.*, **B61**, (2000), 4827; *J. Phys.: Condens. Matter*, **12**, (2000), 8623.

[21] L. Zhang, H. J. Xie, and C. Y. Chen, *Chin. J. Phys.*, **41**, (2003), 148.

[22] J. J. Shi, *Phys. Rev.*, **B68**, (2003), 165335.

[23] J. J. Shi, X. L. Chu, and E. M. Goldys, *Phys. Rev.*, **B70**, (2004), 115318.

[24] B. C. Lee, K. W. Kim, M. Dutta, and M. A. Stroscio, *Phys. Rev.*, **B56**, (1997), 997; *Phys. Rev.*, **B58**, (1998), 4860.

[25] J. Gleize, M. A. Renucci, J. Frandon, and F. Demangeot, *Phys. Rev.*, **B60**, (1999), 15985.

[26] S.M. Komirenko, K.W. Kim, M.A. Stroscio, and M. Dutta, *Phys. Rev.*, **B59**, (1999), 5013.

[27] L. Zhang, J. J. Shi, and T. L. Tansley, *Phys. Rev.*, **B71**, (2005), 245324.

[28] R. Loudon, *Adv. Phys.*, **13**, (1964), 423.

[29] L. Wendler, R. Haupt, and V.G. Grigoryan, *Physica*, **B167**, (1990), 91.

[30] J. Gleize, F. Demangeot, J. Frandon, M. A. Renucci, M. Kuball, B. Daudin, and N. Grandjean, *Phys. Status Solidi (a)*, **183**, (2001), 157; J. Gleize, J. Frandon, F. Demangeot, M. A. Renucci, M. Kuball, J. M. Hayes, F. Widmann, and B. Daudin, *Mater. Sci. Eng (b)*, **82**, (2001), 27.